JOURNAL OF SPACECRAFT AND ROCKETS
Vol. 29, No. 1, January-February 1992

Prediction of Radiant Energy Forces on the TOPEX/POSEIDON Spacecraft

Peter G. Antreasian* and George W. Rosborough†
University of Colorado, Boulder, Colorado 80309

The largest nongravitational forces that will be acting on the TOPEX satellite will be those due to incident and emitted radiation on the spacecraft surfaces. In order to minimize the effects of these forces on orbit determination, a detailed model is being developed so that they may be predicted accurately. This model requires a precise description of the spacecraft shape and orientation, an evaluation of the solar and Earth radiation impinging on the surfaces, and a determination of the radiation being emitted from the surfaces as they heat and cool throughout the orbit. The TRASYS software system is used to evaluate the solar and Earth radiation (albedo and infrared) striking each surface of the spacecraft. This software has been modified to include an Earth radiation model that follows the seasonal variations in albedo and infrared radiation. The SINDA software system is then used to determine the transient temperatures of the spacecraft surfaces. Orbital thermal histories of significant features are given. These temperatures are used to determine the force exerted on each surface due to thermal emission. The emission forces are combined with the incident radiation forces to determine the total force acting on the satellite.

Nomenclature

A	= area
a	= albedo
c	= speed of light
c_0,c_1,c_2	= seasonal albedo constants
$D(f)$	= diffuse angular distribution law
dA	= elemental area
$d\omega$	= solid angle
E	= emissive power
F	= force vector
f	= force per unit mass
G	= radiant flux density, W/m^2
I	= intensity
k	= iteration number
k_0,k_1,k_2	= seasonal emissivity constants
m	= number of radiant energy sources
m_{sc}	= mass of spacecraft
n	= number of surfaces
$\hat{n}$	= unit normal of surface element
P	= power
r	= distance between Earth element $dA_\oplus$ and spacecraft
$\hat{s}$	= radiant energy unit vector
T	= transformation matrix
T	= temperature
t	= time
$\hat{u}$	= unit vector
α	= absorptivity
β	= specularity coefficient
β'	= angle between sun vector and orbit plane
β'_0	= maximum β' angle where spacecraft remains in fixed yaw
γ	= angle between $dA_\oplus$ unit normal and r
ϵ	= emissivity
θ	= angle between $\hat{n}$ and $\hat{s}$
ρ	= reflectivity
σ	= Stefan-Boltzmann constant
Φ	= solar array pitch angle
ϕ	= latitude of Earth element
Ψ	= yaw angle
Ω	= orbit angle from orbit sunrise
$\omega_\oplus$	= orbital rate of Earth

Subscripts

A	= solar array fixed
B	= blackbody or body fixed
b	= back
D	= diffuse
f	= front
I	= incident
O	= orbit fixed
o	= initial
P	= pitch
S	= specular
Y	= yaw
ϵ	= spacecraft emissive energy
$\odot$	= Sun
$\oplus$	= Earth
$\oplus_a$	= Earth albedo
$\oplus_\epsilon$	= Earth emissivity

Superscripts

ir	= infrared spectrum
s	= solar spectrum

Introduction

THE seasonal variations of the world's ocean circulations and how they influence the Earth's climate will soon be investigated with a high-precision Earth-orbiting altimetric satellite. This project, referred to as the Ocean Topography Experiment/Poseidon Mission (TOPEX/POSEIDON), is a joint venture between NASA and the French Centre National d'Etudes Spatiales (CNES). The TOPEX/POSEIDON spacecraft (s/c) will be equipped with two radar altimeters (1 USA and 1 French), which will measure the ocean surface topography.

By measuring the height of a satellite above the ocean surface with the use of a radar altimeter and subtracting the satellite's height in geocentric coordinates, the sea level in

Presented as Paper 90-2895 at the AIAA Astrodynamics Conference, Portland, OR, Aug. 20-22, 1990; received Dec. 26, 1990; revision received Aug. 13, 1991; accepted for publication Aug. 15, 1991.
Copyright © 1990 by the American Institute of Aeronautics and Astronautics, Inc. All rights reserved.

*Doctorate Candidate, Aerospace Engineering Sciences. Member AIAA.
†Assistant Professor, Aerospace Engineering Sciences. Member AIAA.

geocentric coordinates is calculated. Then subtracting this value from the geoid will give the ocean dynamic topography.[1] The knowledge of the dynamic topography is very important in that it consists mainly of surface geostrophic currents and tides that influence global weather patterns.

The TOPEX s/c will orbit the Earth at an altitude of 1336 km, an inclination of 66 deg and a nearly zero eccentricity. The period of the orbit is 1.87 h and its ground trace will repeat every 10 days. TOPEX is expected to be launched in June of 1992 from the European Space Agency's Ariane launch vehicle.

Since the orbit of TOPEX is essentially the reference frame from which the measurements are taken, any error in determining the satellite's position will affect the accuracy of the altimetric measurements. In order to obtain measurements to the degree of accuracy that is required by the scientific community for oceanographic studies, the orbit of the TOPEX s/c must be determined over contiguous 10-day periods, to within 13-cm rms accuracy in the radial component with less than 5-cm rms geographically correlated error.[2] Orbit determination of this accuracy has never before been achieved for an altimetric satellite. At the 1336-km altitude, above any significant influence of the atmosphere, solar radiation pressure is the greatest nongravitational perturbing force on the s/c. In addition to direct radiation from the Sun, the Earth's albedo and infrared (IR) emissions along with IR emissions of the s/c itself will perturb the orbital motion. All of these effects need to be better understood to ensure that the science objectives of the TOPEX/POSEIDON mission can be successfully fulfilled.

Background

Radiant energy effects on the orbital motion of satellites became of interest to celestial mechanicians during the pioneering missions of the Vanguard I and Echo I satellites. Unmodeled acceleration residuals between their observed and computed orbits led Musen et al.,[3] Musen,[4] Parkinson et al.,[5] Shapiro and Jones,[6] and Muhleman et al.[7] to derive simple solar radiation pressure models. Eventually, models were developed to explain the energy and momentum received by satellites from the exposure to Earth reflected sunlight. Dennison[8] computed the illumination of a s/c's surface by numerically integrating the diffusely reflected solar radiation from the Earth over the illuminated portion of the hemisphere. Levin[9] added to this and computed the vectorized components of the illumination on a spherical s/c and displayed the relative magnitudes of the radial and transverse components as a function of s/c position with respect to the sun vector and altitude. Wyatt[10] constructed a variety of terrestrial radiation models (albedo and infrared) in order to see if the force caused appreciable secular changes in the orbital elements, particularly in the orbital period and eccentricity. Wyatt[10] considered the reflection of sunlight off the Earth to be partly diffuse and partly specular. But he concluded that since a satellite is rarely exposed to pure specular reflection from calm waters, the specular Earth reflection effects can be ignored, and since he had assumed either constant or latitudinal symmetric infrared models, the contribution of the infrared radiation on the orbital effects is negligible. However, he states that more realistic models may reveal observable perturbations.

Recent analysis of the Lageos satellite orbit has revealed an unmodeled semimajor axis decay corresponding to an average along-track acceleration that is modulated by several long periodic terms. Several authors, Lautmann,[11] Anselmo et al.,[12] Sehnal,[13] Barlier et al.,[14] Rubincam,[15] and Knocke et al.,[16] have re-examined the effects of radiation pressure on satellite orbits, particularly Lageos. The radiation models now include latitudinal and seasonal dependent Earth radiation, satellite thermal infrared radiation, and more. Anselmo et al.[12] propose that the unexplained long-periodic along-track perturbations of Lageos could be explained by the seasonal variable albedo asymmetry between the northern and southern Earth hemispheres. Anselmo et al.,[12] state that there is no averaging out of the Earth reflected radiation pressure on satellites because of the spatial and temporal variability of the Earth's albedo: "The s/c receives a kick forward before entering the shadow and a kick backward after exiting the shadow."[12] However, since the albedo between the subsatellite points at the entry and exit latitudes may have significantly different mean albedos, the effect does not cancel itself. Sehnal[13] describes the Earth infrared radiation as a spherical harmonic of zeroth- and second-degree zonal terms. He concludes that this effect may contribute to some long-periodic effects in argument of perigee and the ascending node, whereas semimajor axis, eccentricity, and inclination do not suffer secular perturbations. Barlier et al.[14] also compute the effects due to anisotropic thermal emissions of Lageos. Barlier et al.[14] agree with Anselmo et al.[12] that asymmetric Earth reflected radiation between entry and exit points of the eclipse can account for 1050- and 560-day harmonics in the acceleration residuals. Furthermore, Barlier et al.[14] add that anisotropic thermal emissions might not average out over long periods because of eclipses, so that these effects may contribute to the acceleration residuals.

Georgevic[17,18] and Porter[19] developed detailed solar radiation pressure models for spacecraft of complex shape. These models account for the magnitude and direction of the force on each significant vehicle surface. Moreover, these models include the specific absorption and reflection properties of each surface. Also, the radiation pressure on cylindrical or parabolic surfaces were computed. For interplanetary missions within the inner solar system, solar pressure becomes an increasingly significant effect on the orbit the closer the spacecraft moves toward the Sun; therefore, Georgevic[17,18] developed radiation force and torque models for the Mariner Venus/Mercury 1973 spacecraft and the Mariner 9 Mars orbiter. Porter[19] derived a detailed solar radiation model for the Global Positioning System (GPS) space vehicle system in order to improve the orbit determination of these satellites.

Study for TOPEX

An analysis of the radiation forces acting on TOPEX has been undertaken. Since a precise thermal radiative model of a s/c is necessarily computationally intensive, it will be required that this detailed model be computed off-line and that a relatively simple or less computative model that closely represents the actual would be used in the precision orbit determination (POD) process. This is especially true when POD becomes operational. Therefore, the goal of this activity is to provide a precise radiative force model of TOPEX, so that the TOPEX POD scientists will have a standard to base their simpler models on.

The detailed evaluation of the radiation forces is dependent on accurately defining the flux that is incident on the various s/c surfaces and the resulting interaction (absorption, reflection). This process is complicated due to the complex shape of TOPEX and the fact that its orientation continually changes with respect to the Earth and Sun. Additionally, the solar array and the Tracking and Data Relay Satellite System (TDRSS) antenna carried by the satellite both articulate with respect to the s/c bus. Consideration also has to be given to the reflective and absorptive properties of the surfaces, which will change with time.

In addition to the effects of incident radiation on the s/c, the surfaces will also radiate due to their heating from the incident flux and also due to internally generated heat that needs to be dissipated. Essential to this research are the Thermal Radiation Analysis System (TRASYS) and the Systems Improved Numerical Differencing Analyzer (SINDA), which were developed at Martin Marietta.[20,21] TRASYS calculates the radiation fluxes from solar, albedo, and Earth IR incident on each surface of the s/c. SINDA computes the transient orbital thermal history of each surface.

The s/c follows a sinusoidal yaw program except when the Sun lies close to the orbital plane whereupon the satellite maintains a fixed yaw orientation.[22] Simultaneously, the solar array continuously pitches to maintain a Sun-pointing direction. Incorporation of the TDRSS antenna orientation is still under development. To determine the radiation forces acting on the satellite, the s/c is correctly oriented for a given orbital location and TRASYS is exercised to determine the incident fluxes on each surface. Once the fluxes on each surface are determined for all locations around a single orbit, the SINDA software is then used to determine the transient temperatures of each surface. These fluxes and temperatures are then converted to resultant forces based on the surface properties and orientation of each surface. An investigation of the degradation of the surface optical properties has not yet been completed, and thus, constant beginning of mission values are used.

Since the emission of radiation contributes momentum to the s/c, the transmission of the altimeter, radiometer, and TDRSS antennas will also impart recoil forces to the s/c. Operating with a peak power of 20 W over a 1.5-m parabolic antenna, the altimeter is the major active transmitter of energy on TOPEX; therefore, an analysis was performed on it to establish an estimate for the magnitude of its recoil force on the s/c. It was determined that the altimeter's recoil force was three orders of magnitude less than the radiation forces, which will be discussed later. Since this effect remains well below the error associated with these radiation models, the recoil forces from active instrument radiators on TOPEX can be neglected in this analysis.

The radiation pressure model to be used in the POD will incorporate a simple rectangular box and solar array (box-wing model) with dimensions akin to TOPEX. The optical properties and areas of each face of the box and array can be estimated a priori by using the method of least squares to fit the box-wing model to this detailed model. In addition, fairly simple exponential heating and cooling models are being developed to account for the temperature variability of the s/c throughout its orbit. These approximate models, not discussed in this paper, will enable a fairly accurate representation of the true radiation pressure without costing extra computer time during the orbit determination.

Sources of Radiant Energy

Radiant Energy of the Sun

The Sun radiates most of its energy between the wavelengths of 0.2 μm in the ultraviolet region to 3.0 μm of the infrared region. Because its energy source is stable, our Sun emits a nearly constant amount of photons per unit of time,[23] varying less than 0.2%. Intercepted by Earth, at a mean distance of 1 AU, this constant time rate of flow of radiant energy per unit area is known as the solar constant or solar irradiance,[24] $G_\odot = 1367.7$ W/m^2. Since the Earth's orbit is eccentric, the solar radiation flux received by the Earth system varies by ± 45.6 W/m^2 throughout its orbit around the Sun.

Radiant Energy of the Earth

Once the Earth receives the Sun's energy, a fraction of the energy is reflected off the land-water-snow-ice-atmosphere system as shortwave energy with wavelengths from 0.2 to 4.0 μm and the remainder is absorbed into the Earth interior. Because of the thermal inertia of the Earth's interior, the energy that is absorbed will later re-emit as longwave infrared radiation (4.0–40.0 μm).

Since the reflective and absorptive properties of the land, oceans, and clouds differ, the energy that is reflected (albedo) varies latitudinally and longitudinally over the irradiated portion of the planet and the emitted infrared energy varies over the entire planet. As such, the albedo and emissivity of the Earth can be approximately represented analytically as a spherical harmonic expansion. It has been determined that the emissivity ϵ and albedo a can be modeled fairly accurately using only first- and second-degree zonal harmonics,[16]

$$a = a_0 + a_1 P_1(\sin\phi) + a_2 P_2(\sin\phi) \tag{1}$$

$$\epsilon = \epsilon_0 + \epsilon_1 P_1(\sin\phi) + \epsilon_2 P_2(\sin\phi) \tag{2}$$

where ϕ is the latitude, and P_1 and P_2 are the first- and second-degree Legendre polynomials, respectively. The coefficients a_0, a_2, ϵ_0, and ϵ_2 are constants, and the first-degree coefficients a_1 and ϵ_1 have a seasonal variation,

$$a_1 = c_0 + c_1 \cos[\omega_\oplus(t-t_0)] + c_2 \sin[\omega_\oplus(t-t_0)]$$

$$\epsilon_1 = k_0 + k_1 \cos[\omega_\oplus(t-t_0)] + k_2 \sin[\omega_\oplus(t-t_0)]$$

where t is the time in question, t_0 is the reference epoch, $\omega_\oplus$ the orbital period of the Earth, and c_0, k_0, c_1, k_1, c_2, and k_2 are constant parameters. This representation accounts for seasonal variations of the albedo and emissivity of the Northern and Southern Hemispheres.

The Earth has been shown to reflect and emit most of its energy in a diffuse manner, and so each elemental Earth area $dA_\oplus$ radiates constant flux over the hemispherical area encompassing $dA_\oplus$.[16] Therefore, as shown in Fig. 1a, the re-

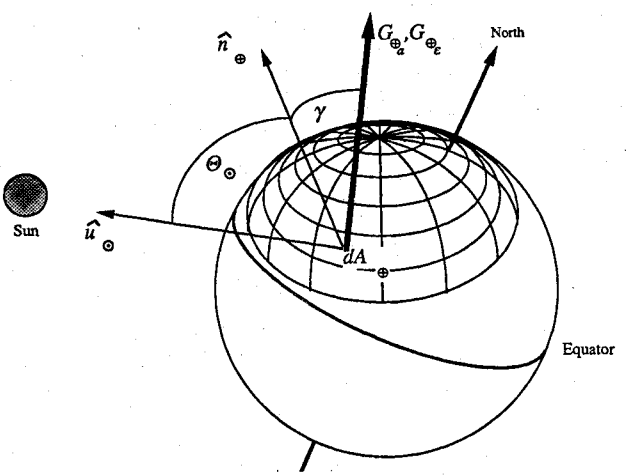

Fig. 1a Earth reflected and emitted energy fluxes.

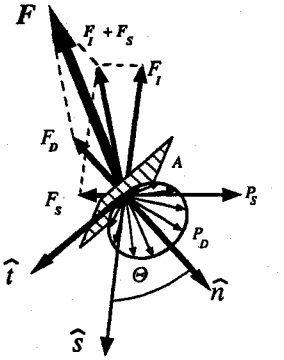

Fig. 1b Resultant force on area A from the incidence, specular, and diffuse reflectance of radiant energy.

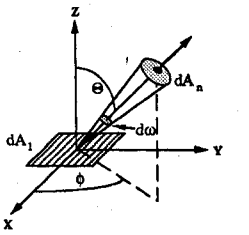

Fig. 1c Elemental surface geometry definition.

flected, radiant energy flux density from an elemental Earth area $dA_\oplus$ irradiating a cross-sectional area on the s/c at a distance r is

$$G_{\oplus_a} = \frac{aG_\odot}{\pi r^2} \cos\theta_\odot \cos\gamma \, dA_\oplus \tag{3}$$

where $\theta_\odot$ is the angle between the unit normal of the elemental Earth area and the unit direction vector to the Sun, and γ is the angle between the unit normal and the directional vector to the satellite. The emitted infrared radiant energy flux density intercepted by a cross-sectional area on the s/c from an elemental Earth area at a distance r (Fig. 1a) is

$$G_{\oplus_\epsilon} = \frac{\epsilon G_\odot}{4\pi r^2} \cos\gamma \, dA_\oplus \tag{4}$$

Radiant Energy of a Heated Surface

If the temperature of a s/c surface is higher than that of its surroundings, such as the surface of a s/c in cold space, then the surface will cool by the release or emission of thermal energy into its surroundings until it achieves thermal equilibrium with its surroundings. Stefan-Boltzmann law states that for a blackbody the rate at which thermal energy is emitted per unit area from the surface, referred to as emissive power, is

$$E_B = \sigma T^4 \tag{5}$$

where σ is the Stefan-Boltzmann constant (5.670×10^{-8} W/m^2 K^4), and T is the temperature of the surface. It should be noted that thermal energy emission is assumed to be diffuse and to obey Lambert's cosine law (discussed later). With the assumption that the ith surface of a s/c behaves like that of a gray body, which means that it emits a constant fraction of the energy spectrum of a blackbody at equal temperature, then the radiant energy flux leaving a heated surface is

$$G_i = \epsilon_i \sigma T_i^4 \tag{6}$$

where ϵ_i is the emissivity of the ith surface.

Reflectivity Models

The reflectivity of a surface depends on the dielectric constant, conductivity, permittivity, and the magnetic permeability of the material and of free space. For this analysis, these parameters are assumed to be constant with respect to time. The reflectivity of a surface is also a function of the wavelength of the incident radiant energy, thus reflectivity can differ between the shorter and longer wavelengths of electromagnetic energy. Therefore, we divide the reflectivity parameter into two spectral bandwidths: 1) the solar reflectivity (visible and uv wave bands), and 2) the IR reflectivity. Furthermore, since most s/c surfaces exhibit a combination of specular and diffuse reflectances, these reflectivities are divided into a diffuse part and a specular part. In the IR wave band, we assume gray surface properties, which says that the absorptivity of the surface is equal to its emissivity.

The surface properties for each surface of a s/c include the absorptivity α, emissivity ϵ, infrared specular reflectivity ρ^{ir}, and solar specular reflectivity ρ^s, such that the absorption and reflectivity for a given surface should add,

$$\alpha^s + \rho_D^s + \rho_S^s = 1.0 \tag{7}$$

$$\alpha^{ir} + \rho_D^{ir} + \rho_s^{ir} = 1.0 \tag{8}$$

assuming the transmissivity is zero. Here, the D and S subscripts refer to diffuse and specular, respectively. It should also be noted that

$$\alpha^{ir} = \epsilon \tag{9}$$

A percentage of the reflectivity is specular and the rest is diffuse such that

$$\rho = \rho_S + \rho_D \tag{10}$$

where

$$\rho_S = \rho\beta \tag{11}$$

$$\rho_D = \rho(1 - \beta) \tag{12}$$

where β refers to the specularity, or percentage of reflected radiation that reflects in a specular manner, and

$$\rho = \rho^{ir} = 1 - \epsilon \tag{13}$$

for the infrared solar spectrum, or

$$\rho = \rho^s = 1 - \alpha \tag{14}$$

for the solar spectrum.

Radiant Energy Force on a Spacecraft

The rate at which the radiant energy is incident or emitted from a flat plate area A per unit time is referred to as energy flux or power. If $\hat{s}$ is the direction of propagation, θ is the angle between the normal $\hat{n}$ of A, and $\hat{s}$ is

$$\cos\theta = \hat{n} \cdot \hat{s} \tag{15}$$

then the power of the incidental radiant energy is dependent on the area A intercepting it,

$$P_I = GA \cos\theta \tag{16}$$

and G is the incidental radiation flux density (W/m^2) from the Sun, Earth albedo surface element, or Earth IR surface element. Because electromagnetic energy delivers a time rate of change of momentum on an elemental surface area dA proportional to its power divided by the speed of light c,

$$\frac{dM}{dt} \propto \frac{P}{c} \tag{17}$$

the force imparted on a flat plate surface resulting from the incidental flux is (see Fig. 1b)

$$F_I = -\frac{P_I \hat{s}}{c} \tag{18}$$

Substituting Eq. (16),

$$F_I = -(1/c)GA \cos\theta \hat{s} \tag{19}$$

The reflected energy is expressed as a combination of the two extreme cases of specular and diffuse energy. Assuming that the reflectivity, specularity, and diffusivity are uniform over the entire area, the flux or power of the reflected energy will then be

$$P_S = \beta\rho GA \cos\theta \tag{20}$$

for the specular energy, and

$$P_D = (1 - \beta)\rho GA \cos\theta \tag{21}$$

for the diffuse energy. The part of the light energy that reflects specularly, also shown in Fig. 1b, exerts a force,

$$F_S = -(1/c)\beta\rho GA \cos\theta(2 \cos\theta\hat{n} - \hat{s}) \tag{22}$$

Diffusely emitted energy results in some fraction of the power contributing to a normal force on the surface and the remainder contributing to a shear force. For symmetric diffusion, the shear force will be zero. The normal force of the diffusely reflected energy, as shown in Fig. 1b, is then

$$F_D = -(1/c)D(f)(1-\beta)\rho G \cos\theta \hat{n} \tag{23}$$

A flat plate surface of area A with temperature T emits diffuse IR radiation with a total power of

$$P_\epsilon = \epsilon\sigma T^4 A \tag{24}$$

Therefore, the normal force resulting from the diffuse emission of long-wave IR energy is

$$F_\epsilon = -\frac{D(f)}{c}\epsilon A\sigma T^4 \hat{n} \tag{25}$$

The term $D(f)$ is less than 1 and represents the fraction of the diffuse power [Eq. (21) or (24)] emitted normal to the surface. The actual value of $D(f)$ will depend on the angular distribution of the diffuse energy. For a surface obeying Lambert's cosine law of diffuse emission, $D(f)$ will be 2/3 [the derivation of $D(f)$ for Lambert's cosine law is given in the following subsection].

Now adding the incident, diffuse, and specular reflected forces, as demonstrated in Fig. 1b,

$$F = F_I + F_S + F_D \tag{26}$$

the total radiation force acting upon a flat plate from the exposure to sunlight or terrestrial radiation is

$$F = -(1/c)GA\cos\theta\{(1-\rho\beta)\hat{s} + [D(f)(1-\beta)\rho + 2\rho\beta\cos\theta]\hat{n}\} \tag{27}$$

Essentially, the exterior of the s/c can be divided into many flat plates, even cylindrical and parabolic features can be adequately subdivided into elemental flat plate areas. Therefore, the forces due to incident, reflected, and emitted radiation acting on each outer surface of the TOPEX s/c are calculated independently for each radiant energy source, then all are summed together in a body-fixed reference frame,

$$F_T = \sum_{i=1}^{n}\left(F_{\epsilon_i} + \sum_{j=1}^{m} F_{ij}\right) \tag{28}$$

where n is the number of surfaces, and m refers to the incident radiation sources.

Lambert's Cosine Law and the Diffuse Radiant Energy Force

When an elemental area dA is described as being perfectly diffuse, it implies that the surface behaves as an isotropic radiator. In other words, the surface radiates uniformly in all directions. The radiance N, which is defined as the radiant energy flux (power) per unit area per unit solid angle, for such a surface is constant and, therefore, independent of direction. The radiant intensity I, on the other hand, is described as the radiant energy power (flux) per solid angle. In the eighteenth century, J. H. Lambert postulated that the radiant intensity I entering $d\omega$ from the diffusely radiating surface decreases from the maximum I_0 along the normal of dA as the cosine of the angle Θ between the normal $\hat{n}$ and the direction of the measurement $\hat{r}$

$$I = I_0 \cos\Theta \tag{29}$$

This relation is known as Lambert's cosine law; a surface obeying this law is said to be Lambertian (purely diffuse reflector and emitter). It will be shown that 2/3 of the diffuse radiant energy flux emitted from dA is responsible for imparting a force normal to the surface. To visualize this, imagine that diffuse radiant energy from dA (as in Fig. 1c) subtends a solid angle $d\omega$,

$$d\omega = \frac{dA_n}{r^2} \tag{30}$$

and intercepts another area dA_n at a distance r

$$dA_n = r^2 \sin\Theta\, d\Theta\, d\phi \tag{31}$$

where ϕ is the azimuthal angle.

In order to compute the total flux (power) P of the diffuse radiant energy leaving dA, integrate the radiant intensity over the hemisphere σ, encompassing dA,

$$P_D = \int_\sigma I\, d\omega = \int_0^{2\pi}\int_0^{\pi/2} I_0 \cos\Theta \sin\Theta\, dA\, d\Theta\, d\phi \tag{32}$$

which becomes

$$P_D = \pi I_0 \tag{33}$$

The force imparted on dA from the release of diffuse energy is

$$F_D = -\frac{P_D D(f)}{c}\hat{n} \tag{34}$$

where the factor $D(f)$ accounts for the fact that only a fraction of the power is emitted normal to the surface.

Integrating the intensity times the normal component of the unit direction vector $\hat{r}$ over the hemisphere, the diffuse radiation force is

$$F_D = -\frac{1}{c}\int_0^{2\pi}\int_0^{\pi/2} I(\hat{r}\cdot\hat{n})\hat{n}\sin\Theta\, d\Theta\, d\phi = -\frac{1}{c}\int_0^{2\pi}\int_0^{\pi/2} I_0\cos^2\Theta\sin\Theta\, d\Theta\, d\phi\hat{n} \tag{35}$$

which becomes

$$F_D = -\frac{2}{3}\frac{\pi I_0}{c}\hat{n} \tag{36}$$

By comparing with the previous expression for the diffuse force [Eq. (34)], the angular distribution coefficient is

$$D(f) = 2/3 \tag{37}$$

Therefore, 2/3 of the power released from dA contributes to the diffuse force.

Yaw and Pitch Routines

As shown in Fig. 2, the orientation of the body-fixed coordinate frame (x_B, y_B, z_B) within the s/c body is such that it originates at the center of mass of the vehicle with the positive y axis pointing opposite of the solar array axis, the positive z axis is nadir Earth pointing, and the positive x axis pointing orthogonal to the y and z axes. The origin of the orbit-fixed frame (x_O, y_O, z_O) coincides with the s/c's center of mass, and the positive z axis is coincident with the z axis of the body-fixed frame, but the positive y axis points opposite of the orbital angular momentum vector of the orbit, and the x axis points orthogonal to the y and z axes. This orbit-fixed coordinate system can also be described as the RTN (radial, transverse, normal) orbit-fixed frame, where radial is nadir (Earth pointing), normal is perpendicular to the plane (opposite of the orbital angular momentum vector), and transverse is or-

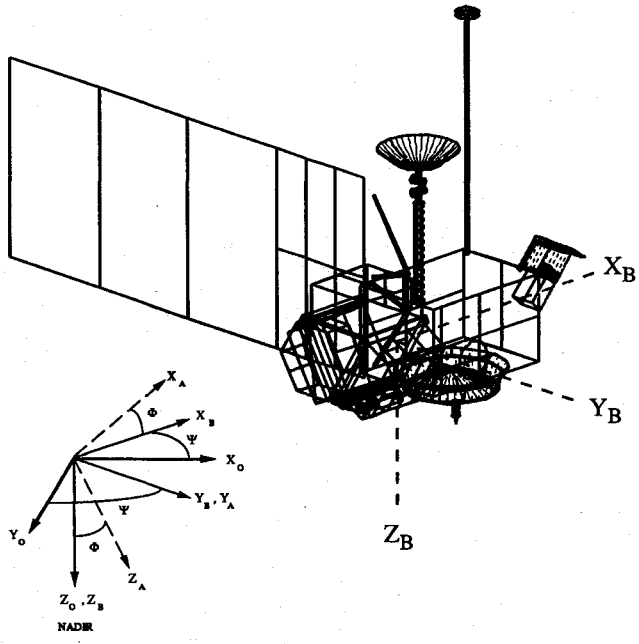

Fig. 2 310-node TRASYS model of TOPEX with the spacecraft coordinate systems.

thogonal to radial and normal. The attitude of the TOPEX s/c is to be controlled by a sinusoidal yaw program, and the pointing of the solar array toward the Sun is to be guided by a pitch routine, both developed by Fairchild Space Company (FSC).[22] The sinusoidal yaw routine is defined by

$$\begin{aligned} \beta' \geq \beta_0': &\quad \Psi = 90 \text{ deg} + (90 \text{ deg} - \beta') \cos \Omega \\ 0 \text{ deg} < \beta' < \beta_0': &\quad \Psi = 0 \text{ deg} \\ -\beta_0' < \beta' < 0 \text{ deg}: &\quad \Psi = 180 \text{ deg} \\ \beta' \leq -\beta_0': &\quad \Psi = -90 \text{ deg} - (90 \text{ deg} + \beta') \cos \Omega \end{aligned} \tag{38}$$

where β' refers to the angle between the Earth-Sun vector and the plane of the orbit, Ω is the orbit angle measured from orbit sunrise, β_0' the maximum angle of β' where the s/c will remain in a fixed yaw orientation, and Ψ the yaw angle rotated positively from x_O about the satellite to Earth vector. Orbit sunrise occurs when the s/c, moving toward the Sun, crosses the plane orthogonal to the Earth-Sun direction.

The solar array pitch angle is specified by,

$$\Phi = 180 \text{ deg} + \tan^{-1}\left[\frac{\sin \Omega \cos \beta'}{\cos \Phi \cos \Omega \cos \beta' - \sin \Psi \sin \beta'}\right] \tag{39}$$

where the pitch angle Φ, which rotates positively from x_B about the satellite body-fixed y axis, orients the cell side of the solar array toward the Sun for optimum Sun pointing.

The force on each surface of the s/c is first computed in the satellite body-fixed coordinate frame, then as the s/c orbits about the Earth, the sinusoidal yaw routine, described earlier, will rotate the craft about the orbit-fixed/body-fixed z axis. In order to compute the forces on the s/c in the orbit-fixed frame, they must be rotated from the body-fixed frame to the orbit-fixed frame by way of the yaw steering rotational transformation matrix,

$$T_Y = \begin{bmatrix} \cos \Psi & -\sin \Psi & 0 \\ \sin \Psi & \cos \Psi & 0 \\ 0 & 0 & 1 \end{bmatrix} \tag{40}$$

where Ψ is the yaw angle defined earlier. Thus, the transformation from the body-fixed frame to the orbit-fixed frame is

$$\hat{u}_O = T_Y \hat{u}_B \tag{41}$$

here $\hat{u}_B$ is the unit vector of a force imparted onto a surface in the body-fixed frame, and $\hat{u}_O$ is the unit vector of that force in the orbit-fixed frame. In addition to the yaw routine, the solar array must pitch to correctly point its face to the Sun. The forces imparted onto the solar array must be rotated from a solar array-fixed coordinate frame to the body-fixed frame and finally to the orbit-fixed frame. The solar array-fixed frame (x_A, y_A, z_A), shown in Fig. 2, is oriented at the center of the solar array with the x axis pointing normal to the cell side of the array and the y axis pointing along the rotational axis into the s/c's body; the z axis is then orthogonal to the x and y axes. To transform each force to the body-fixed frame, the force that is defined in the solar array-fixed frame by the unit vector $\hat{u}_A$ is rotated about the body-fixed y axis. This is represented by

$$\hat{u}_B = T_P \hat{u}_A \tag{42}$$

where the rotational pitch transformation matrix is

$$T_P = \begin{bmatrix} \cos \Phi & 0 & \sin \Phi \\ 0 & 1 & 0 \\ -\sin \Phi & 0 & \cos \Phi \end{bmatrix} \tag{43}$$

and Φ is the pitch angle defined earlier. Now the yaw transformation matrix must be used to transform these forces from the body-fixed to the orbit-fixed coordinate frame; thus, by combining the two rotations into one equation,

$$\hat{u}_O = T_Y T_P \hat{u}_A \tag{44}$$

This provides the necessary transformation for expressing the solar array-fixed forces in the orbit-fixed frame.

Software Systems

The computation of the radiant energy fluxes incident on the s/c is very rigorous, especially since the s/c changes its orientation with respect to the radiant sources of the Sun and Earth throughout its orbit. Some surfaces of the vehicle will be exposed while others will be shadowed. In addition, the solar array pitches to track the Sun while the s/c yaws about its Earth pointing axis. Fortunately, an extensive computer software system, TRASYS,[20] was developed by Martin Marietta to compute the radiant energy fluxes incident upon each surface of a s/c throughout its orbit. A detailed thermal heat transfer model of the thermal emissions from the TOPEX s/c can be computed with the incorporation of the SINDA[21] also created by Martin Marietta as an industry standard approved by NASA.

TRASYS calculates the radiation fluxes from solar, albedo, and Earth IR incident on each surface of the s/c, the absorbed heat rates for each surface, and the radiation conductors between each surface. The s/c's exterior surface geometry, orbit parameters, orientation, and surface properties are entered into the program. Each surface of the s/c is represented within individual block coordinate systems by rectangles, polygons, discs, cylinders, spheres, and cones and then is related to a central body-fixed coordinate frame. TRASYS outputs the radiative flux densities from the Sun and the Earth as well as from reflected surfaces. It also outputs the absorbed heat arrays with respect to time and the radiation conductors from surface to surface. The absorbed heat arrays contain the total radiative energy per unit time absorbed by each surface at each point in the orbit. And the radiation conductors consist of the fraction of the total energy emitted from surface i that would be absorbed by surface j at each point in the orbit.

This system allows up to 1000 surfaces or nodes to be defined for the s/c. TRASYS takes each exposed surface and divides it into many elemental areas to calculate the integrated flux density on the surface.

SINDA is a software system that solves both steady-state and transient lumped-parameter (resistance-capacitance) heat transfer problems using finite differencing techniques. The thermal model of the s/c is composed of a three-dimensional array of nodal surfaces such as those in TRASYS, plus interior nodes that describe the thermal properties of the materials and electronics. Each node represents either a radiation conductor or a linear conductor. In a finite differencing model, these conductors are also called boundary and diffusion nodes, respectively. The inputs for SINDA consist of the absorbed heat arrays and radiation conductors described as outputs from TRASYS, linear conductors between nodes, thermal capacitances of diffusion nodes, internal heat model or duty cycles of instruments and power plants, and logic for the thermal radiative louver blades. SINDA outputs the temperature vs time histories of each node or surface. Besides performing a steady-state analysis SINDA can perform several transient analyses, such as forward or forward-backward finite differencing schemes. In the forward finite differencing scheme, a heat balance equation is written about a diffusion node that uses only temperature derivatives at the current time to predict the overall temperature change. The equation can be solved explicitly for temperatures at later times. In the forward-backward finite differencing scheme one equation is written about a diffusion node as a forward finite differencing equation and another as a backward finite differencing equation. The sum of the two equations is the forward-backward implicit equation. It uses the average of the temperature derivatives at current and next times to predict the overall temperature change.

TOPEX Spacecraft Model

The s/c contractor, Fairchild Space Company, has provided s/c definitions that consist of both the TRASYS and SINDA models. A preliminary TRASYS s/c model consisted of 186 surfaces, but improvements of the s/c design and attention to finer detail have improved this model; now the TRASYS model consists of 310 surfaces. The current SINDA transient thermal model includes over 500 nodes. In the near future, a final set of models will be delivered corresponding to the as-built s/c. Figure 2 shows the 310-node representation of the satellite modeled in the TRASYS software. For each surface, normal vectors, areas, absorptivity, and emissivity of the surface coatings are defined. The SINDA thermal model of TOPEX also includes radiation conductors to space and between exterior or interior surfaces, linear conductors between materials, thermal capacitances of the diffusion nodes, an internal heat model, which represents the duty cycles of the electronics, and a louver logic algorithm, which represents the opening and closing of the louvers depending on the temperatures. Radiation conductors are considered the most important source of heat transfer within the s/c; however, contact between two conducting surfaces could also be important in some cases. Heat transfer by convection is considered to be negligible in the s/c. Therefore, a model containing these radiation conductors along with important linear conductors give a near accurate description of the thermal history of TOPEX throughout its orbit. SINDA calculates the temperatures at each node on the s/c and thus gives a indication of the thermal gradient on the s/c. Because each surface reradiates proportional to T^4, an indication of the forces generated by thermal imbalances will be given.

A few assumptions have been made in computing the TOPEX radiant energy force model. These include circular orbit; constant beginning of mission surface properties; diffuse reflection and emission obey Lambert's cosine law for angular distribution of energy; the contribution of the force due to the specular surface-to-surface reflections is negligible; cylindrical Earth shadow model; and all components of the s/c reflect the same percentage of reflected energy specularly. The last assumption is due to the fact that these data are not yet available for each surface coating.

The values of the various parameters used to compute this model are listed in Tables 1–4. Table 1 lists current universal constants for the force computations: solar flux, speed of light, and Earth radius and gravitational constant. Table 2 lists TOPEX's orbital parameters. The 310-node s/c model parameters, which include mass, surface properties, the specular reflectivity coefficient, and fixed yaw region, as well as the projected areas are given in Table 3. The area-to-mass ratio of TOPEX will change throughout its mission because of its changing orientation and fuel expenditure; therefore, Table 3 lists the maximum and minimum ratios for the start of the mission. Table 4 shows the latest known surface properties of the various surface coatings.

Results

Radiation Forces

The incident, reflected, and emitted radiation forces acting on each surface were computed. These were then summed to get the total force acting on the s/c at each point in the orbit. For the case when the angle between the Sun and the plane of

Table 1 Force modeling constants

Speed of light, c	299,792,458 m/s
Solar constant, $G_\odot$	1367.70 W/m^2
Earth radius, $R_\oplus$	6,378,137 m
Earth cylindrical shadow radius, R_s	6,402,000 m
Gravitational parameter of Earth, $\mu_\oplus$	$3.98600448 \times 10^{14}$m^3/s^2

Table 2 Orbit parameters

Inclination, i	66 deg
Eccentricity, e	0.00
Altitude, h	1336.000 km
Nodal precession rate, $\dot{\Omega}$	− 2.31 deg/day
Period, P	112 min

Table 3 310-node spacecraft model

Number of surfaces, n	310
Spacecraft mass, m_{sc}	2500.0 kg
Specular reflectivity coefficient (all surfaces), β	0.20
Diffuse angular distribution function, $D(f)$	2/3
Fixed-yaw region, $-\beta\dot{0} < \beta' < \beta\dot{0}$, $\beta\dot{0}$	15 deg
x_B projected s/c body area, A_x	4.70 m^2
y_B projected s/c body area, A_y	8.18 m^2
z_B projected s/c body area, A_z	8.30 m^2
Solar array area, A_s	25.5 m^2
Maximum area-to-mass ratio, $(A/m)_{max}$	0.140 cm^2/g
Minimum area-to-mass ratio, $(A/m)_{min}$	0.019 cm^2/g

Table 4 Beginning of mission surface properties

Surface coating	α	ϵ
Front of solar array	0.79	0.81
Back of solar array	0.18	0.85
Silver Teflon	0.07	0.76
Silver Teflon (ITO)[a]	0.15	0.76
MLI[b] black Kapton	0.85	0.80
MLI aluminum Kapton	0.45	0.80
White paint	0.18	0.85
Black paint	0.98	0.98
Gold plate	0.08	0.15

[a]ITO = indium tin oxide.
[b]MLI = multilayer insulation.

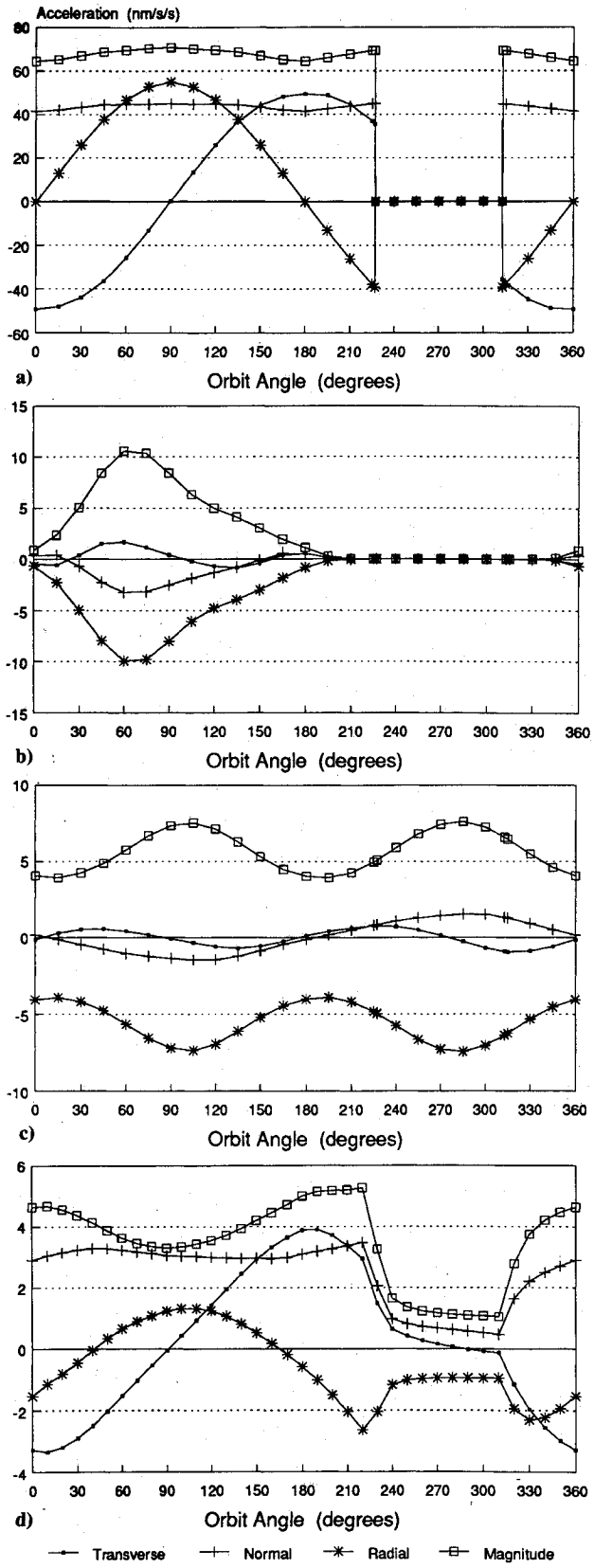

Fig. 3 Radiation force per unit mass histories for $\beta' = 40$ deg: a) direct solar radiation; b) Earth albedo radiation; c) Earth infrared radiation; d) spacecraft thermal infrared emissions.

the orbit β' is 40 deg, Figs. 3 and 4 show the resultant radiation forces per unit mass inferred from the solar, Earth albedo, Earth IR, s/c emitted IR, and the total radiant energy acting on TOPEX as represented by the 310-node model. The three components of the force shown correspond to the RTN orbit-fixed frame described earlier.

The magnitude of the solar radiation force in Fig. 3a ranges from 0 nm/s^2 during occultation to 71 nm/s^2 near orbit noon (corresponding to the Sun being highest in the sky with respect to the s/c local horizon). Much of this force is due to the large area of the solar array which tracks the Sun throughout the orbit ($f_{\text{array}} \approx 53$ nm/s^2). The force history due the Earth's albedo reflections on the s/c is shown in Fig. 3b. The magnitude of this force ranges from 0 nm/s^2 during occultation to 11 nm/s^2 before orbit noon. The skewness of this plot about orbit noon is mainly the result of the asymmetric albedo between the Northern and Southern Hemispheres. Figure 3c shows the force history on TOPEX due to the Earth's infrared emissions. The sinusoidal nature of this plot is the result of the pitch rotation of the solar array; the magnitude ranges from 4 to 8 nm/s^2. The s/c's thermal emissive force history is represented in Fig. 3d, and the magnitude ranges from 0.3 nm/s^2 when the temperature of the s/c has cooled down during occultation to 6 nm/s^2 near the end of the solar heating. Finally, the total resultant force ($f_{\text{solar}} + f_{\text{albedo}} + f_{\text{ir}} + f_{\text{s/c}}$) on the 310-node model of TOPEX is shown in Fig. 4. The magnitude of the total radiation force per unit mass ranges from 7 to 79 nm/s^2.

The magnitudes of each radiation force will vary as β' changes due to the orbit's changing orientation with respect to the Sun. The magnitude will also change as the Earth's reflectivity and emissivity change throughout the year. Furthermore, the s/c remains in a fixed-yaw orientation at low β' angles, and for $\beta' > 56$ deg, the s/c experiences no occultation. Table 5 compares the maximum magnitudes of the force per unit mass for three orbit configurations: 1) $\beta' = 0$ deg, when the Sun is in the orbit plane, 2) $\beta' = 40$ deg, and 3) $\beta' = 88$ deg, when the s/c is in full sunlight and the Sun lies close to the angular momentum vector.

Table 6 gives the accelerations of each radiation effect in terms of an equivalent thermal energy imbalance. An acceleration of 1.0 nm/s^2 refers approximately to an energy imbalance of 750 W.

Spacecraft Temperatures

In order to compute the transient temperatures on the s/c surfaces, SINDA iterates nearly 30 orbital revolutions until the solution relaxes and the transient temperatures of each surface stabilize,

$$|T_i(k-1) - T_i(k)| < 0.001 \text{ K} \qquad (45)$$

where k is the iteration number. Figures 5a-5c display the thermal orbital history of a few surfaces during one orbit for the $\beta' = 40$ deg case. The transient temperature signature of the cell side and backside of the solar array during one orbit is shown in Fig. 5a. Always Sun-pointing, the temperature rises

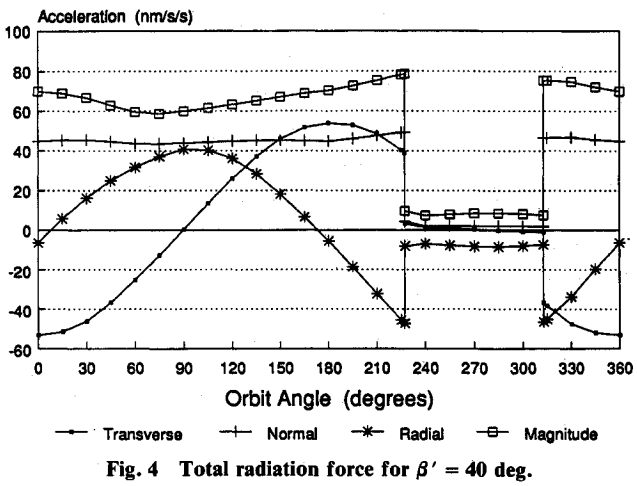

Fig. 4 Total radiation force for $\beta' = 40$ deg.

Table 5 Maximum magnitude of forces (nm/s²) for different orbit orientations

Case	β', deg	Solar, f_{solar}	Albedo, f_{albedo}	Earth IR, f_{ir}	S/C IR, $f_{s/c}$	Total without S/C IR, f_{T_1}	Total, f_{T_2}
1	0	73	12	10	5	74	78
2	40	71	11	8	6	74	79
3	88	65	2	5	6	66	71

Table 6 Maximum energy imbalances for the $\beta' = 40$ deg case

Radiant energy	Power, W
Solar	53,300
Albedo	8,250
Infrared	6,000
S/C infrared	4,500

exponentially to a maximum at 345 K, then it rapidly cools with an exponential decay to a temperature of 240 K. The difference between the front and back temperatures reaches approximately 15 K. Figure 5b shows the orbital history of the instrument module (IM), which is the central rectangular box in Fig. 2. One node facing each positive and negative axis of the body-fixed coordinate frame was chosen to represent the variation of the orbital temperatures of TOPEX. It should be noted that other nodes along the same directions may differ significantly. The $-z$ face of the IM heats up to approximately 368 K, and since no Earth radiation impinges on it, the surface cools down to 115 K. The temperatures of the $+x$ and y faces remain close to 200 K, because they see very little or no direct radiation. The influence of the Earth's radiation on the s/c surface is illustrated by the thermal history of the $+z$ (Earth-facing) surface. Here the temperature averages around 280 K, except just before entering and after exiting the Earth's shadow where this face receives a brief burst of sunlight. In addition, the infrared influence is shown by the shallow temperature decline during the shadow, whereas the albedo effect is shown by the slight rise and decay of the temperature around orbit noon. Figure 5c shows thermal histories for one node on each the altimeter ($+z$), propulsion module (PM) ($-x$), and the $+y$, $+z$ modular power system (MPS) louver (without sunscreen). The PM points toward the Sun throughout most of the sunlit portion of the orbit, and so the temperature averages around 330 K during this time. As the temperature of the interior of the s/c rises, the louver radiator opens its blades wider. Its effects on stabilizing the interior temperature is shown in this figure.

To get an idea of what gives rise to higher thermal force magnitudes, the thermal force derived from the imbalance of thermal energy released on any axis can be computed as follows:

$$f = -\frac{2}{3c}\frac{A}{m_{sc}}\sigma(\epsilon_f T_f^4 - \epsilon_b T_b^4) \tag{46}$$

Table 7 lists approximations of the thermal forces on the s/c in a body-fixed coordinate frame to illustrate the temperature

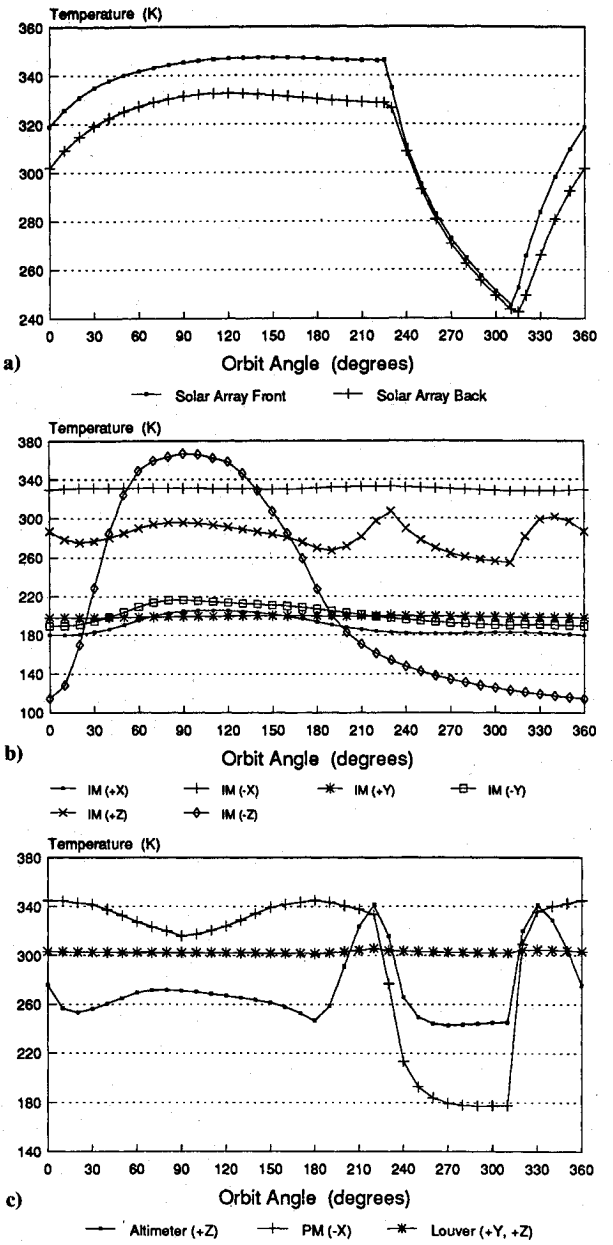

Fig. 5 Orbital thermal histories during $\beta' = 40$ deg: a) the Solar Array; b) the instrument module (IM); c) the altimeter, propulsion module (PM), and radiative louver.

Table 7 Thermal force on each body-fixed axis of TOPEX, $\beta' = 40$ deg

Face	Sun or shadow	Area, m²	T_f, K	T_b, K	ϵ_f	ϵ_b	Power, W	f, nm/s²
Solar array	Sun	25.5	350	335	0.81	0.85	1400	−1.86
x axis	Sun	4.70	328	188	0.80	0.80	1460	−1.95
y axis	Both	8.19	200	205	0.80	0.80	−41.2	0.05
z axis	Sun	8.30	293	365	0.80	0.80	−2620	3.49
z axis	Shadow	8.30	275	130	0.80	0.80	1364	−1.81
x + array	Sun	30.2	—	—	—	—	2860	−3.81
z + array	Sun	33.8	—	—	—	—	4020	−5.35

differential T^4 effect across the front and back sides of each axis of the body, the solar array, and the solar array and body combined. The z axis is shown to have the greatest thermal imbalance, whereas the y axis has the least imbalance because this axis is always perpendicular toward the Sun, so that the solar array remains Sun pointing.

Conclusions

To assist TOPEX precision orbit determination, a detailed model of the radiative forces acting on the TOPEX s/c has been constructed. The effects due to solar, Earth albedo, Earth infrared emissions, and the s/c's thermal emissions are all being considered. A precise description of the spacecraft provided by Fairchild Space Company is being utilized in conjunction with the TRASYS and SINDA software systems in order to obtain as precise as possible prediction of these forces.

The effect of solar radiation on the spacecraft is by far the largest of the radiation effects. Although this effect is routinely modeled in precision orbit determination work, the results of the detailed model indicate it will be necessary to model this effect on TOPEX with some degree of fidelity. This is primarily due to the area variations of the spacecraft body as it yaws in order to maintain the solar array in Sun pointing configuration. Also, due to the sinusoidal yaw program that the satellite follows, the array does not point perfectly normal to the Sun, resulting in a significant force component not aligned with the Sun direction.

Albedo and infrared radiation effects are approximately 10% of those of the direct solar radiation. These forces have a very characteristic twice per revolution signature due to the pitching of the solar array with respect to the nadir direction. Although these forces are unlikely to significantly degrade the accuracy of TOPEX orbit determination, minimal modeling (constant area for the spacecraft body and a pitching flat plate for the solar array) will substantially reduce their effect and remove them as a potential error source.

The effect of thermal emissions of the spacecraft surfaces has been found to be of the same magnitude as the Earth infrared radiation effect. Thermal emission forces due to surfaces on the spacecraft body are found to be approximately twice the size of the emission force due to the solar array. However, until test data are obtained to validate the predicted surface temperatures, it is impossible to state with any certainty the level of modeling detail that will be required for these forces in the orbit determination process.

Radiation forces (incident and emitted) acting on the TOPEX spacecraft are the largest nongravitational force acting on the satellite. By utilizing these precise models of the radiation forces it will be possible to minimize the degrading effect of these forces on precision orbit determination. In turn, this will aid in fulfilling the TOPEX/POSEIDON mission objectives.

Acknowledgments

This research was supported under Jet Propulsion Laboratory Contract 957388. The authors wish to thank Carl Jensen of Martin Marietta for his advice and consultation on the TRASYS and SINDA software systems. The authors also wish to thank William Schreiner of the University of Colorado for programming assistance and the thermal modeling group at Fairchild Space Company for the TRASYS and SINDA models of TOPEX.

References

[1]Anon., "TOPEX/POSEIDON Mission Description," Jet Propulsion Lab., Pasadena, CA, D-601, Rev. B, Dec. 1985, p. 2.1.

[2]Stewart, R., Fu, L.-L., and Lefebvre, M., "Science Opportunites from the TOPEX/Poseidon Mission," Jet Propulsion Lab., Pasadena, CA, Pub. 86-18, July 1986, p. 25.

[3]Musen, P., Bryant, R., and Bailie, A., "Perturbations in Perigee Height of Vanguard I," *Science,* Vol. 131, March 25, 1960, pp. 935,936.

[4]Musen, P., "The Influence of Solar Radiation Pressure on the Motion of an Artificial Satellite," *Journal of Geophysical Research,* Vol. 65, No. 5, 1960, pp. 1391–1396.

[5]Parkinson, R. W., Jones, H. M., and Shapiro, I. I., "Effects of Solar Radiation Pressure on Earth Satellite Orbits," *Science,* Vol. 131, March 25, 1960, pp. 920,921.

[6]Shapiro, I. I., and Jones, H. M., "Perturbations of the Orbit of the Echo Balloon," *Science,* Vol. 132, Nov. 18, 1960, pp. 1484–1486.

[7]Muhleman, D. O., Holdridge, D. B., Carpenter, R. L., and Oslund, K. C., "Observed Solar Pressure Perturbations of Echo I," *Science,* Vol. 131, Nov. 1960, p. 1487.

[8]Dennison, A. J., Jr., "Illumination of a Space Vehicle Surface Due to Sunlight Reflected from Earth," *American Rocket Society Journal,* Vol. 32, No. 4, 1962, pp. 635–637.

[9]Levin, E., "Reflected Radiation Received by an Earth Satellite," *American Rocket Society Journal,* Vol. 32, No. 9, pp. 1328–1331.

[10]Wyatt, S. P., "The Effect of Terestrial Radiation Pressure on Satellite Orbits," *Dynamics of Satellites Symposium,* edited by M. Roy, Academic, New York, 1963, pp. 180–196.

[11]Lautmann, D. A., "Perturbations of a Close-Earth Satellite Due to Sunlight Diffusely Reflected from the Earth II: Variable Albedo," *Celestial Mechanics,* Vol. 16, 1977, pp. 3–25.

[12]Anselmo L., Farinella, P., Milani, A., and Nobili, A. M., "Effects of the Earth-Reflected Sunlight on the Orbit of LAGEOS Satellite," *Astronomy and Astrophysics,* Vol. 117, 1983, pp. 3–8.

[13]Sehnal, L., "Effects of the Terrestrial Infrared Radiation Pressure on the Motion of an Artificial Satellite," *Celestial Mechanics,* Vol. 25, 1981, pp. 169–179.

[14]Barlier, F., Carpino, M., Farinella, P., Mignard, F., Milani, A., and Nobili, A. M., "Non-Gravitational Perturbations on the Semimajor Axis of LAGEOS," *Annales Geophysicae,* Vol. 4, No. A3, 1986, pp. 193–210.

[15]Rubincam, D. P., "On the Secular Decrease in the Semimajor Axis of LAGEOS's Orbit," *Celestial Mechanics,* Vol. 26, 1982, pp. 361–381.

[16]Knocke, P. C., Ries, J. C., and Tapley, B. D., "Earth Radiation Pressure Effects on Satellites," *Proceedings of the AIAA/AAS Astrodynamics Conference,* AIAA Paper 88-4292, Washington, DC, Aug. 1988, pp. 577–586.

[17]Georgevic, R. M., "Mariner Venus/Mercury 1973 Solar Radiation Forces and Torques," Jet Propulsion Lab., Pasadena, CA, JPL TM33-698, Dec. 1974.

[18]Georgevic, R. M., "The Solar Radiation Pressure on the Mariner 9 Mars Orbiter," Jet Propulsion Lab., Pasadena, CA, JPL TM33-582, Dec. 1972.

[19]Porter, W. W., "Solar Force-Torque Model for the GPS Space Vehicle System," Rockwell International, Space Division, Downey, CA, Jan. 1979.

[20]Jensen, C., "Thermal Radiation Analysis System TRASYS II User's Manual," ANSI Version 1.0, Martin Marietta Aerospace Corp., Denver, CO, Feb. 1987.

[21]Jensen, C., "Systems Improved Numerical Differencing Analyzer and Fluid Integrator, SINDA '85 User's Manual," Version 2.1, Martin Marietta Aerospace Corp., Denver, CO, Nov. 1987.

[22]Perrygo, C., "TOPEX Satellite Yaw Maneuvers," Fairchild IOC REF: 968:SE:87-074, Fairchild Space Co., Germantown, MD, Nov. 1987.

[23]Kivelson, M. G., *The Solar System, Observations and Interpretations,* Vol. IV, Prentice-Hall, Englewood Cliffs, NJ, 1986, pp. 17-19.

[24]Willson, R. C. and Hudson, H. S., "Solar Luminosity Variations in Solar Cycle 21," *Nature,* Vol. 332, 1988, pp. 810–812.

Paul F. Mizera
Associate Editor